Available online at www.sciencedirect.com
ScienceDirect
Solar Energy Materials & Solar Cells 92 (2008) 864–872
Solar Energy Materials and Solar Cells
www.elsevier.com/locate/solmat

Photoreduction of CO_2 to fuels under sunlight using optical-fiber reactor

The-Vinh Nguyen[1], Jeffrey C.S. Wu*

Department of Chemical Engineering, National Taiwan University, Taipei 10617, Taiwan, ROC

Received 24 September 2007; received in revised form 10 January 2008; accepted 20 February 2008
Available online 18 April 2008

Abstract

An optical-fiber reactor is employed to photocatalytically reduce CO_2 with H_2O to fuels under UVA artificial light and concentrated natural sunlight. The optical fiber is coated with gel-derived TiO_2–SiO_2 mixed oxide-based photocatalysts. Fe atom is found to insert into the TiO_2–SiO_2 lattice during sol–gel process, resulting in the full visible light absorption as well as the effect on product selectivity of the derived catalyst. Under UVA, ethylene is mainly produced on Cu–Fe/TiO_2 catalyst with the quantum yield of 0.0235%, whereas Cu–Fe/TiO_2–SiO_2 catalyst is observed to favor methane production with the quantum yield of 0.05%. Meanwhile, the overall energy efficiency is found to be much higher on Cu–Fe/TiO_2–SiO_2 (0.0182%) than on its Cu–Fe/TiO_2 counterpart (0.0159%). There is only methane evolved over both bare TiO_2–SiO_2 and Cu–Fe/TiO_2–SiO_2 catalysts under natural sunlight with the production rates of 0.177 and 0.279 μmol/g-cat h, respectively. For the former catalyst, the increase in light intensity is not found to compensate the inherent electron–hole recombination in the TiO_2–SiO_2–acac catalyst, whereas the superior photoactivity of Cu–Fe/TiO_2–SiO_2 catalyst under natural sunlight could be ascribed to its full absorption of visible light.

Keywords: Photocatalytic reduction; TiO_2; Carbon dioxide; Solar energy; Optical fiber

1. Introduction

When sunlight reaches the surface of the Earth, some of it is absorbed and warms the Earth, whereas some sunlight is utilized by green plants to produce hydrocarbons that constitute the world's fossil fuel reserves. Owing to strong development of human activities, consumption of fossil fuel for energy demand dramatically increases worldwide, resulting in the shortage of energy sources for future use. Meanwhile, release of carbon dioxide into the atmosphere by burning of these fossil fuels is observed to substantially increase from the last century, which causes global warming along with related serious issues [1]. In order to save the Earth as well as to maintain the sustainable development of human being, CO_2-free production of energy is really desirable and is much paid attention by scientists in recent years [2–4]. Among the processes intensively and extensively done in the last decades, photocatalytic reduction of CO_2 into fuels by using natural sunlight is promising to sustainably produce energy. Although there are a large number of studies on the CO_2 reduction to fuels using photocatalysts [5–18], very few researches are known about their activities under natural sunlight. Recently, Guan et al. reported the reduction of CO_2 with H_2O under concentrated sunlight using $K_2Ti_6O_{13}$-based photocatalysts [13,15]. The production rates of main products reported by Guan et al. were very high for H_2 (32.8 μmol/g-cat h) and HCOOH (20.7 μmol/g-cat h), but very low for CH_4 (0.3 μmol/g-cat h) [13].

Our motivation is to seek photo-driven chemical reactions using solar energy directly. The ideal is to use highly focused sunlight to accelerate a photoreaction, so that mass production of chemicals is viable. Sunlight can be collected using a focus device, and transmitted to an optical-fiber reactor, which provides an economical way to deliver photons uniformly in a reaction zone. In this present work, we employ gel-derived TiO_2–SiO_2 mixed

*Corresponding author. Tel.: +886 22363 1994; fax: +886 23632 3040.
E-mail address: cswu@ntu.edu.tw (J.C.S. Wu).
[1]Present address: Faculty of Environment, Hochiminh City University of Technology, Hochiminh City, Vietnam.

0927-0248/$ - see front matter © 2008 Elsevier B.V. All rights reserved.
doi:10.1016/j.solmat.2008.02.010

oxide-based photocatalysts to reduce CO_2 with H_2O to fuels under natural sunlight by using a solar concentrator. Various kinds of metals loaded on TiO_2–SiO_2 mixed oxide along with different catalyst carriers are also used to improve photoactivities.

2. Experimental

2.1. Catalyst preparation

Commercial titanium dioxide powder (P25, Degussa) was used as a TiO_2 source. $Cu(NO_3)_2 \cdot 3H_2O$ and $Fe(NO_3)_3 \cdot 9H_2O$ (Aldrich) were employed as precursors of metal dopants on TiO_2 support. Tetraisopropoxytitanium (TTIP, Merck) and tetraethyl orthosilicate (TEOS, Merck) were used as precursors for TiO_2–SiO_2 mixed oxides. Acetyl acetone (Merck) denoted as acac was employed as a chelating agent during the sol–gel process. The polymer cladding of optical fiber (ET tone Taiwan) was removed by calcination at 500 °C for 3 h. This step was followed by washing off the remained residue with 10 M NaOH aqueous solution and distilled water in ultrasonic bath, 3 times for each.

For the preparation of metal supported TiO_2 thin film, TiO_2 slurry with corresponding metal salts was prepared by the incremental addition of 2 ml of aqueous polyethylene glycol (Merck, average MW of 20,000) solution with the metal salts to 0.5 g of TiO_2 powder in a mortar under vigorous grinding with pestle [19]. Each 0.1 ml of the aqueous polyethylene glycol solution was added after the previous mixture had formed a uniform and lump-free paste. Thus prepared uniform slurry was coated on optical fibers by dip coating method or on glass plates by a doctor-blade technique. After natural drying at room temperature, the thin film was calcined in static air at 450 °C for 30 min.

Synthesis of TiO_2–SiO_2 mixed oxide was carried out in two steps with the schematic diagram of preparation procedures shown in Fig. 1 [20]. The details of the procedures are as follows:

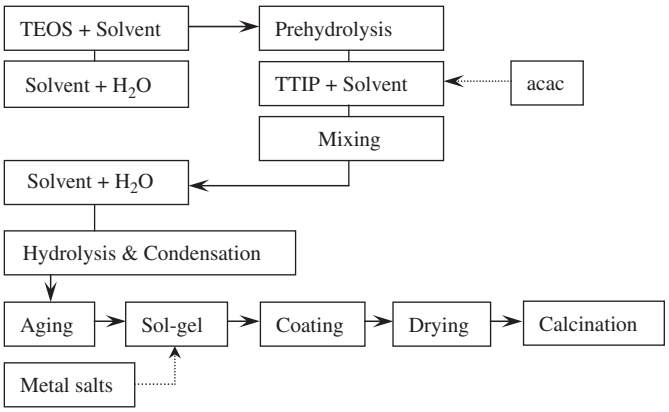

Fig. 1. Schematic diagram of preparation procedures of TiO_2–SiO_2 mixed oxides.

2.1.1. Chemical modification of TTIP

The two solutions were mixed and refluxed at 80 °C for 1 h under vigorous stirring (ca. 1500 rpm) as follows: the first solution consisted of the corresponding volume of chelating agent in 15 ml solvent (50% v/v of ethanol and isopropanol) and the second one was TTIP diluted in 35 ml solvent. The resulted deep yellow transparent liquid (when the acac as a chelating agent was used) or a colorless transparent liquid (without chelating agent) was cooled to ambient temperature for 1 h.

2.1.2. Sol–gel preparation

The hydrolyzant (35% hydrochloric acid and the amount of de-ionized water used to hydrolyze TEOS in 10 ml solvent) was added to TEOS solution (TEOS dissolved in 30 solvent) via a dropping funnel and vigorously stirred at 50 °C for 45 min, which called pre-hydrolysis of TEOS. After that, the modified TTIP as described above was added in the solution under vigorous stirring. After 10 min, the hydrolysis was completed by addition of the residual amount of de-ionized water diluted in 18 ml solvent under vigorous stirring. Finally, 15 ml solvent was introduced after another 10 min had elapsed.

The molar ratio of alkoxides:water:hydrochloric acid:-solvents was 1:4:0.19:5 and the content of SiO_2 in TiO_2–SiO_2 mixed oxides was 5 wt%. The sol–gel solution was aged for 24 h at room temperature and then dried in the oven at 80 °C for 24 h. The resulting xerogel was calcined in static air at 500 °C for 2 h.

The molar ratio of acac/TTIP of 1 was employed to prepare sample TiO_2–SiO_2–acac. The sample prepared without using chelating agent was denoted as TiO_2–SiO_2. For preparation of metal-doped TiO_2–SiO_2, the same synthesis procedure of TiO_2–SiO_2 mixed oxide as described above was employed, except that corresponding metal salts were mixed with the derived TiO_2–SiO_2 sol–gels after the sol–gel processes.

2.2. Characterization

TiO_2 thin films were characterized with X-ray diffraction (XRD, Phillips, Cu-K_α radiation) for crystallinity, scanning electron microscopy with energy dispersive X-ray spectrometer (SEM-EDX, Philips XL30, EDAX DX4) for the film thickness and surface morphology, nitrogen adsorption (Micromeritics ASAP 2000) for the BET specific surface area, pore size and pore volume. The band-gap energies of TiO_2 films were determined by UV–vis diffuse reflectance spectroscopy (UV–vis DRS, Varian Cary 100). The light intensity was measured with a Lumen meter (Exfo). XPS measurements were taken on a VG Microtech MT500 spectrometer, operated with a constant pass energy of 50 eV and with Mg Kα radiation as the excitation source ($hv = 1253.6$ eV). The catalyst was pressed into a pellet, and then adhered on sample holder by a carbon tape. All binding energies were referenced to oxygen (1 s) at 530.7 eV or carbon (1 s) at 285.6 eV. Ti–O–Si

linkage was determined by using FT-IR (Nexus 470, Thermo Nicolet).

Quantum yield (Φ) of the reaction is approximately calculated by using Eqs. (1) and (2). Eight or twelve electrons are required to transform CO_2 to methane or ethylene, respectively. The energy efficiency (η) is estimated by Eq. (3), which represents the conversion of photo to chemical energy:

$$\Phi_{CH_4}(\%) = \frac{8\,\text{mol of methane yield} \times 100\%}{\text{moles of photon absorbed by catalyst}} \quad (1)$$

$$\Phi_{C_2H_4}(\%) = \frac{12\,\text{mol of ethylene yield} \times 100\%}{\text{moles of photon absorbed by catalyst}} \quad (2)$$

$$\eta(\%) = \frac{\text{combustion heat of methane (ethylene)} \times \text{moles of methane (ethylene) yield} \times 100\%}{h\nu \times \text{moles of photon absorbed by catalyst}} \quad (3)$$

where h is Planck constant, v is the frequency of photon, and heat of combustions of methane and ethylene are 802 and 1411 kJ/mol, respectively.

The mole of photon absorbed by catalyst was assumed to be equal to that absorbed by number of optical fibers employed in the reactor. The latter value was estimated on the basis of the outlet energy subtracted from the inlet energy through the optical-fiber reactor [21]. In order to avoid the scattering of light out of the aperture of Lumen meter, the total number of catalyst-coated optical fibers (typically 216) in the reactor were put in one narrow Pyrex glass tube with the diameter of 5 mm and the length same to that of optical fibers (110 mm). A blank measurement of photon absorbed by the Pyrex glass tube without optical fibers was also measured to get the net value of photon absorbed by the number of catalyst-coated optical fibers.

The amount of catalyst coated on carriers including glass plate and optical fiber is determined by the difference between the weight of catalyst-coated carrier and that of bare carrier. Owing to the too small amount of catalyst coated on one optical fiber, the amount of catalyst coated on this carrier is measured on the basis of the total number of optical fibers in the photoreactor, which are 216 fibers.

2.3. Photocatalytic conversion of CO_2 into fuels reaction

Photocatalytic reaction was carried out in a continuous circular Pyrex glass reactor (216 cm^3) with a quartz window for conduction of light irradiation. Catalyst-coated optical fibers were inserted in the reactor in a way such that the light source (high-pressure Hg lamp, 150 W or natural sunlight) can enter along the fibers to conduct the photocatalytic reaction on its surface as shown in Fig. 2(a) [18]. The incident light is split to two beams when hitting the internal surface of fiber, due to the difference of refraction index between the TiO_2 film and the fiber. Part of the light is reflected and transmitted along the fiber, while the rest penetrates and excites the titania layer at the interface. The light gradually spreads and diminishes to the end of the fiber.

The UVA (320–500 nm) light was obtained by using an appropriate color filter (Exfo). In order to determine the photoactivity of catalyst under real sun, natural sunlight was collected by using a solar concentrator (Himawari, Japan). The light intensity was measured on the quartz window with unit of mW/cm^2. The reactor was covered with a heating tape connected to temperature controller with a thermocouple placed at the top of the catalyst bed to maintain the reaction at around 75 °C. The reactor was purged by CO_2 gas bubbling through distilled water for 1 h at 75 °C before and during the reaction. The space velocity of CO_2 gas and H_2O vapor was maintained at 0.72 h^{-1} for every experiment. The outlet gases were analyzed at some periods of time by using GC equipped with FID and porapak Q column.

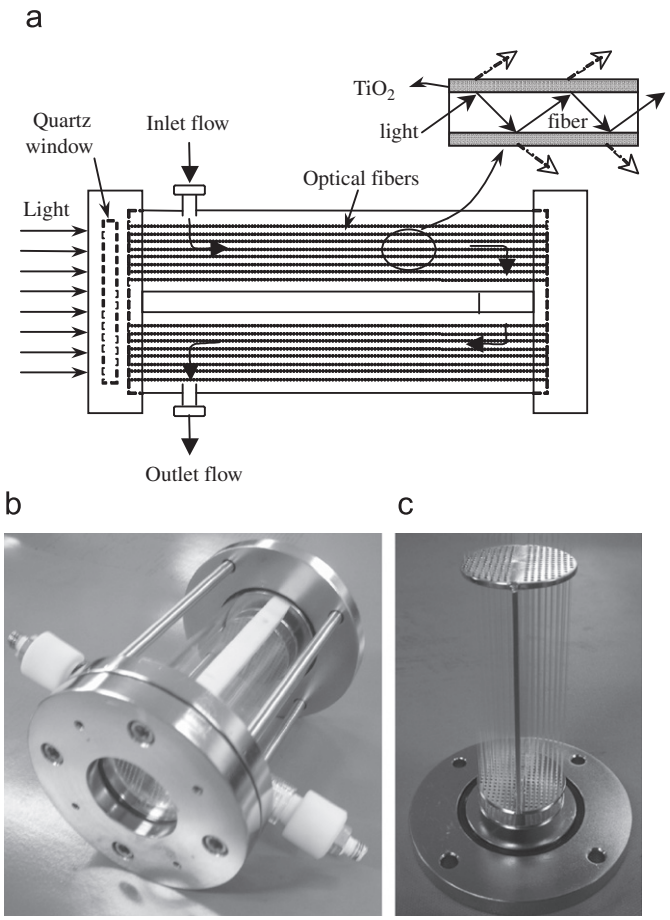

Fig. 2. Schematic diagram (a) and images (b) of photoreactor with catalyst coated optical fibers.

3. Results and discussion

3.1. Catalyst characterization

The specific surface area and band-gap energy of various catalysts are shown in Table 1. The specific surface area of TiO_2–SiO_2 is much higher than that of TiO_2–SiO_2–acac. As TiO_2–SiO_2–acac is loaded with 0.5 wt% of Cu and Fe, its specific surface area is significantly decreased from 119.9 to 44.7 m^2/g. Band-gap energy of Cu (0.5 wt%)–Fe (0.5 wt%)/TiO_2–SiO_2 (2.95 eV) is observed to be slightly decreased in comparison with that of bare TiO_2–SiO_2 (3.30 eV), which is consistent with our previous results [22]. Meanwhile, band-gap energy of Cu (0.5 wt%)–Fe (0.5 wt%)/TiO_2–SiO_2–acac is substantially decreased to 1.55 eV, which is promising to absorb the full range of visible light.

Fig. 3 depicts SEM images of metal-loaded TiO_2 films coated on optical fiber. The thickness of TiO_2–SiO_2-based thin film on optical fiber is around 53 nm. Cracks are observed on the morphological surface of the thin film. This result is probably ascribed to quick evaporation of solvents in the TiO_2–SiO_2 sol–gel solution after dip coating.

The X-ray diffraction patterns of different catalysts as thin films coated on glass plates are shown in Fig. 4. TiO_2–SiO_2, TiO_2–SiO_2–acac and Cu–Fe/TiO_2–SiO_2 catalysts show amorphous phases. Interestingly, as Cu and Fe are doped on TiO_2–SiO_2–acac catalyst, anatase peak is significantly observed. It has been suggested that during the synthesis process Fe ions can be located in octahedral positions of TTIP [23]. Then, after the calcination treatment, when the lattice is already formed it remains in such positions and consequently the anatase structure remains stable [23]. Owing to the function of acac as a chelating agent that depresses the hydrolysis and condensation rates of TTIP, Fe ions can be easily located in octahedral positions of TTIP in comparison with the case of without using chelating agent. Accordingly, the phenomenon of anatase peak appearance on Cu–Fe/TiO_2–SiO_2–acac catalyst is probably due to the inserting of Fe ion into the TiO_2–SiO_2 lattice, which reinforces the regularity of the derived material. As a consequence, the crystallinity of Cu–Fe/TiO_2–SiO_2–acac catalyst is superior as compared to those of bare TiO_2–SiO_2–acac and Cu–Fe/TiO_2–SiO_2 counterparts.

The UV–vis diffuse reflectance spectroscopy of different catalysts depicted in Fig. 5 is measured to elucidate their UV and visible light absorption. TiO_2–SiO_2 obviously

Table 1
Specific surface area and band-gap energy of various catalysts

Photocatalyst	S_{BET} (m^2/g)	E_g (eV)
TiO_2 (P25)	50.0	3.11
TiO_2–SiO_2	145.1	3.30
TiO_2–SiO_2–acac	119.9	3.26
Cu(0.5 wt%)–Fe(0.5 wt%)/TiO_2–SiO_2	39.4	2.95
Cu(0.5 wt%)–Fe(0.5 wt%)/TiO_2–SiO_2—acac	44.7	1.55

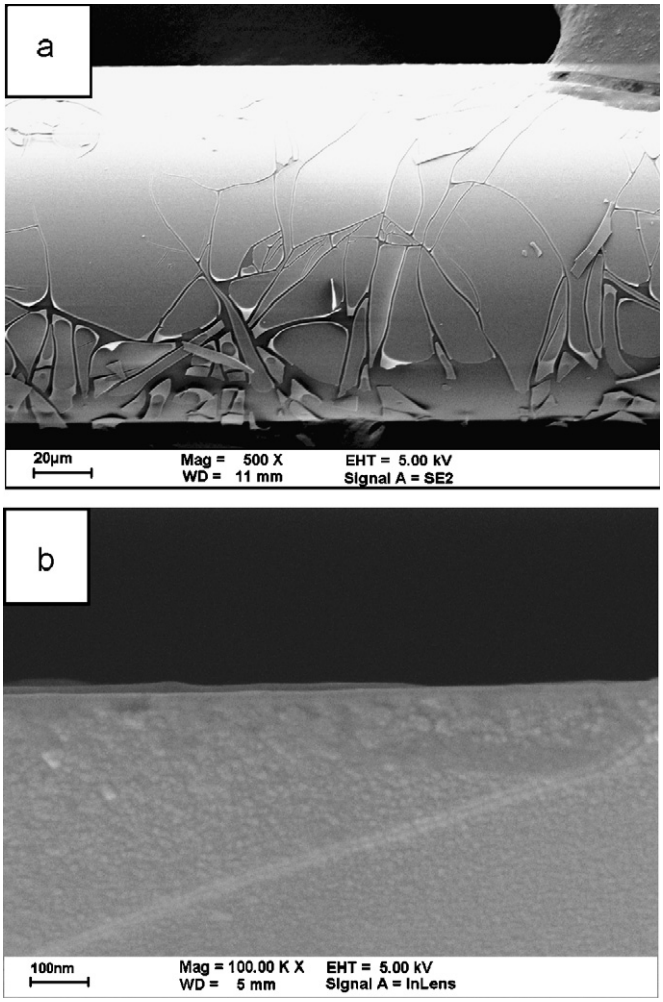

Fig. 3. SEM images of TiO_2–SiO_2 film coated on optical fiber. (a) Surface morphology, and (b) cross-section view.

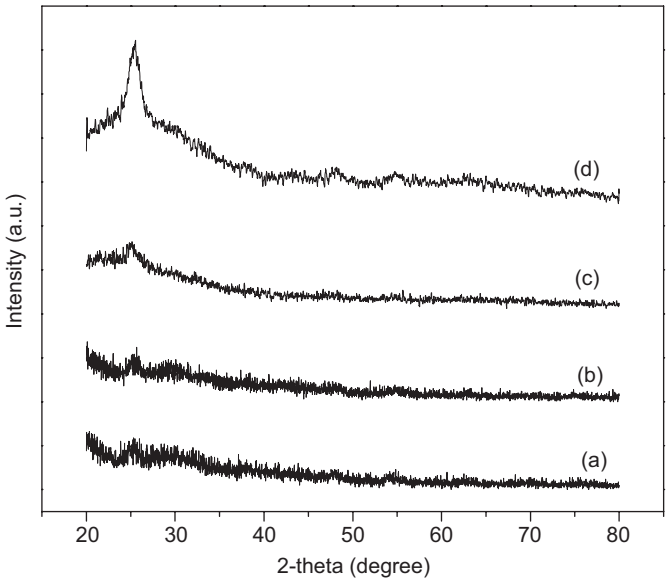

Fig. 4. X-ray diffraction patterns of different catalysts. (a) TiO_2–SiO_2, (b) TiO_2–SiO_2—acac, (c) Cu(0.5 wt%)–Fe(0.5 wt%)/TiO_2–SiO_2, and (d) Cu(0.5 wt%)–Fe(0.5 wt%)/TiO_2–SiO_2–acac.

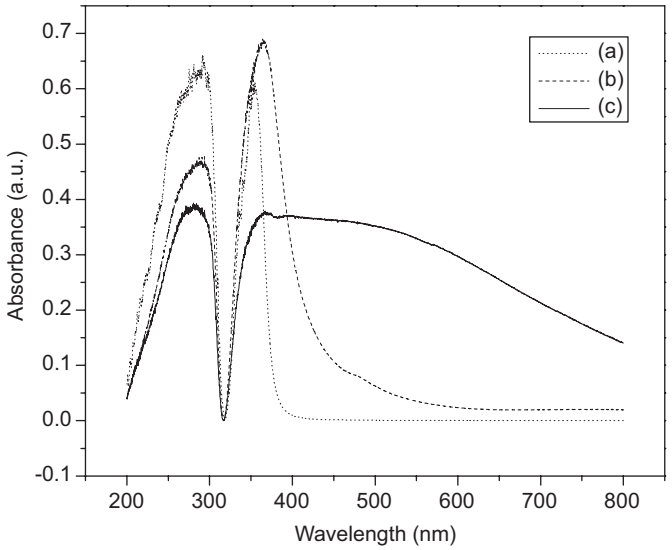

Fig. 5. UV–vis spectroscopy of different TiO_2–SiO_2 mixed oxide thin films. (a) TiO_2–SiO_2, (b) Cu(0.5 wt%)–Fe(0.5 wt%)/TiO_2–SiO_2, and (c) Cu(0.5 wt%)–Fe(0.5 wt%)/TiO_2–SiO_2–acac.

presents UV light absorption as shown in Fig. 5a. Meanwhile, Cu–Fe/TiO_2–SiO_2 appears to extend its absorption spectrum to visible light of 550 nm wavelength (Fig. 5b), which is consistent with our previous report of Cu–Fe/TiO_2 catalyst. This result could be due to the visible light absorption of iron oxides with their band-gap energies of 2.0–2.3 eV [24]. On the other hand, when Cu and Fe are doped on TiO_2–SiO_2–acac, the derived catalyst becomes gray and is observed to fully absorb visible light as shown in Fig. 5c. This result could be ascribed to the effect of partial substitution of Ti and Si by Fe ion in the catalyst lattice. In Fig. 5a sharp decrease of absorption band near 320 nm is due to the background subtraction of glass plate (SiO_2).

Figs. 6a and b show the XPS spectra of Cu 2p and Fe 2p on Cu–Fe/TiO_2–SiO_2 catalyst, respectively. Binding energy of Cu $2p_{3/2}$ is measured at 931.9 eV, which could be assigned to Cu(I) oxidation state [25]. Meanwhile, Fe $2p_{3/2}$ depicts the binding energy at around 710.8 eV, indicating the main presence of Fe^{3+} oxidation state on catalyst [25]. Ti 2p XPS spectra on TiO_2–SiO_2–acac and Cu(0.5 wt%)–Fe(0.5 wt%)/TiO_2–SiO_2–acac catalysts are shown in Fig. 7. Binding energy of Ti $2p_{3/2}$ on TiO_2–SiO_2–acac is ca. 459.3 eV. When Cu and Fe is added to TiO_2–SiO_2, the binding energy of Ti $2p_{3/2}$ of resulting catalyst is measured at 459.8 eV. A positive shift of 0.5 eV binding energy could be ascribed to the substitution of Ti ions by Fe counterparts in the TiO_2–SiO_2 lattice.

3.2. Photocatalytic conversion of CO_2 into fuels

In this study, Cu–Fe/TiO_2–SiO_2 catalysts are observed to photoreduce CO_2 with H_2O to various kinds of products that include significant amount of ethylene and methane as well as trace amount of ethane and methanol. The reactor

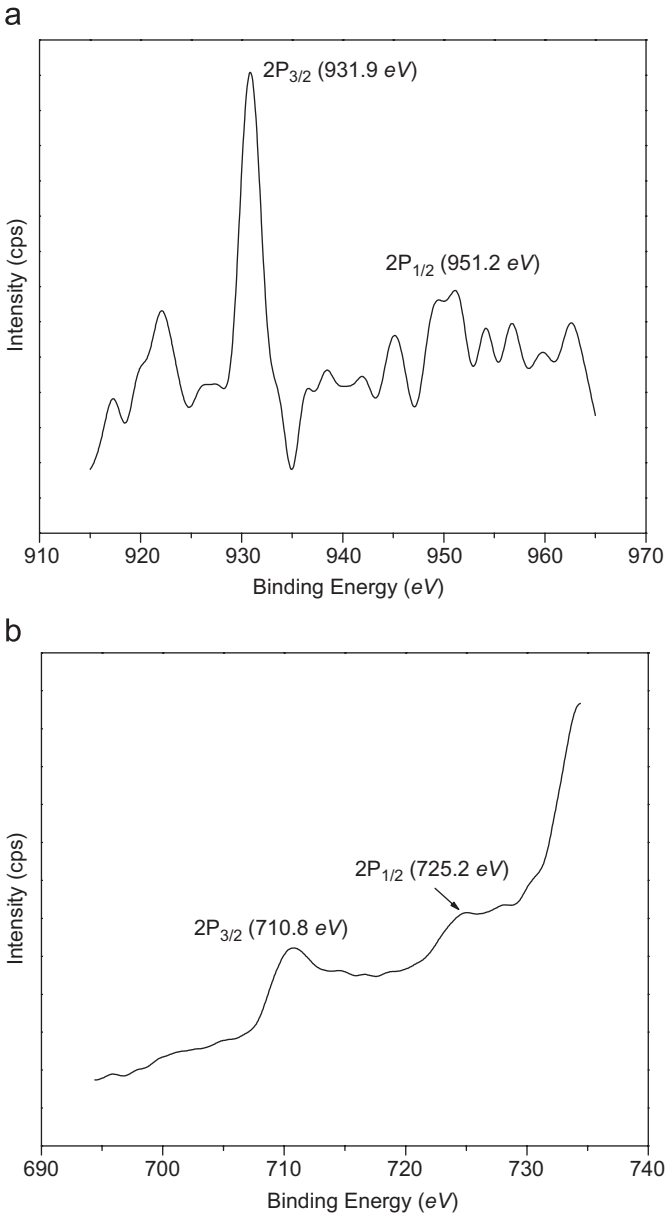

Fig. 6. XPS spectroscopy of Cu(0.5 wt%)–Fe(0.5 wt%)/TiO_2–SiO_2–acac catalyst. (a) XPS spectrum of Cu 2p and (b) XPS spectrum of Fe 2p.

is covered with a heating tape to maintain the reaction at around 75 °C to assure that all of light hydrocarbons could reach the GC detector. Consequently, there is no hydrocarbon as a liquid-phase product observed by naked eyes in the reactor after the photocatalytic reaction. Furthermore, owing to high redox potentials of long-chain hydrocarbons, the photoreduction of CO_2 with H_2O over Cu–Fe/TiO_2–SiO_2 catalysts to these products is impossible under UVA light and natural sunlight in Taipei, Taiwan.

Table 2 presents production rate of methane and ethylene over various kinds of catalysts under UVA. Methane is observed to evolve over all of catalysts in which the maximum production rate of methane, 1.860 μmol/g-cat h is measured on Cu(0.5 wt%)–Fe(0.5 wt%)/TiO_2–SiO_2–acac catalyst coated over optical fiber. Meanwhile ethylene is

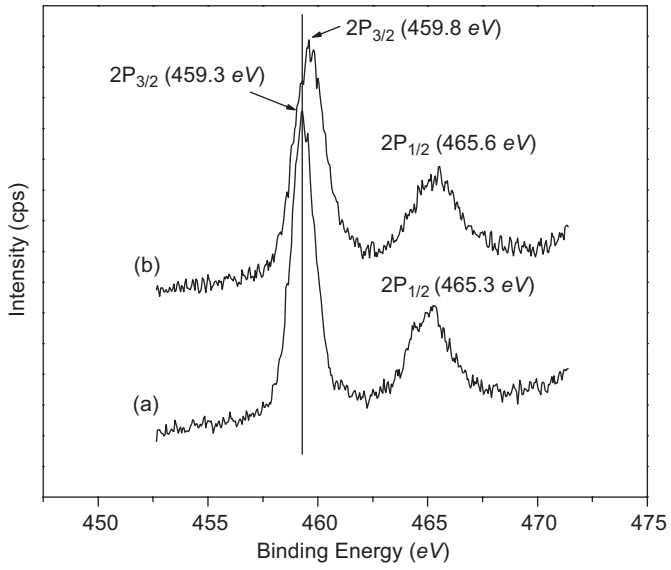

Fig. 7. XPS spectra of Ti 2p of (a) TiO_2–SiO_2–acac and (b) Cu(0.5 wt%)–Fe(0.5 wt%)/TiO_2–SiO_2–acac catalyst.

Table 2
Production rate of methane and ethylene over various catalysts under UVA

Photocatalyst[a]	Ethylene production rate (μmol/g h)[b]	Methane production rate (μmol/g h)[b]
TiO_2/glass plate	0	Trace
TiO_2–SiO_2/glass plate	0	0.043
TiO_2–SiO_2–acac/optical fiber	0	0.185
Cu(0.5 wt%)–Fe(0.5 wt%)/TiO_2/glass plate	0.486	0.060
Cu(0.5 wt%)–Fe(0.5 wt%)/TiO_2/optical fiber	0.575	0.914
Cu(0.5 wt%)–Fe(0.5 wt%)/TiO_2–SiO_2/glass plate	0.415	0.153
Cu(0.5 wt%)–Fe(0.5 wt%)/TiO_2–SiO_2–acac/glass plate	0.540	0.103
Cu(0.5 wt%)–Fe(0.5 wt%)/TiO_2–SiO_2–acac/optical fiber	0.211	1.860

[a]TiO_2–SiO_2 was synthesized by sol–gel process with 5 wt% of SiO_2; acac stands for the acetyl acetone as a promoter during the preparation process of TiO_2–SiO_2.

[b]Methane and ethylene production rate was determined on the basis of average production rate after the reaction time of 4 h. The irradiation source was in UVA range (320–500 nm) with the intensity of 225 mW/cm^2.

only produced on catalysts doped with Cu and Fe metals. The largest production rate of ethylene, 0.575 μmol/g-cat h is observed on Cu(0.5 wt%)–Fe(0.5 wt%)/TiO_2 coated over optical fiber.

In order to efficiently utilize real sunlight for photoreduction of CO_2 to fuels, solar concentrator is employed to conduct sunlight into the reactor. The production rate of methane over TiO_2–SiO_2 mixed oxide-based catalysts under natural sunlight on some specific days are depicted

Table 3
Production rate of methane over TiO_2–SiO_2 mixed oxide-based catalysts under natural sunlight[a]

Photocatalyst[b]	Methane production rate (μmol/g.h)[c]
TiO_2–SiO_2–acac/optical fiber	0.177[d]
Cu(0.5 wt%)–Fe(0.5 wt%)/TiO_2–SiO_2–acac/optical fiber	0.279[e]

[a]Natural sunlight was obtained by using the solar concentrator as illustrated in the experimental section.

[b]TiO_2–SiO_2 was synthesized by sol–gel process with 5 wt% of SiO_2; acac stands for the acetyl acetone as a promoter during the preparation process of TiO_2–SiO_2.

[c]Methane production rate was determined on the basis of average production rate after the reaction time of 4 h.

[d]Experiment for TiO_2–SiO_2–acac catalyst was carried out on May 11, 2007 from 9.30 am to 3.00 pm in Taipei, Taiwan under average solar light intensity of 6.35 mW/cm^2.

[e]The experiment for Cu(0.5 wt%)–Fe(0.5 wt%)/TiO_2–SiO_2–acac was carried out on May 12, 2007, from 10.30 am to 4.00 pm under average solar light intensity of 2.05 mW/cm^2.

in Table 3. When optical fiber is used as a catalyst carrier, methane evolution is higher on Cu(0.5 wt%)–Fe(0.5 wt%)/TiO_2–SiO_2–acac catalyst (0.279 μmol/g-cat h) than that on bare TiO_2–SiO_2–acac counterpart (0.177 μmol/g-cat h). Because natural sunlight is dependent on the weather of the day when the experiment is carried out, photoactivities of catalysts towards hydrocarbon production could be compared one another provided that the intensity of sunlight were same for everyday. Nevertheless, the average intensity of natural sunlight used to photocatalytically reduce CO_2 on TiO_2–SiO_2–acac catalyst was 6.35 mW/cm^2 on May 11, 2007 from 9.30 am to 3.00 pm in Taipei, Taiwan. Meanwhile, photoreduction of CO_2 on Cu(0.5 wt%)–Fe(0.5 wt%)/TiO_2–SiO_2–acac catalyst was carried out on May 12, 2007, from 10.30 am to 4.00 pm under average sunlight intensity of 2.05 mW/cm^2. These results imply that the addition of Cu and Fe metals on TiO_2–SiO_2–acac catalyst significantly improve the photoactivity of resulting catalyst towards methane production under solar light.

Table 4 presents the quantum yield (Φ) and energy efficiency (η) of ethylene and methane production over different catalysts under UVA. The quantum yield and energy efficiency of ethylene and methane production are observed comparable on Cu(0.5 wt%)–Fe(0.5 wt%)/TiO_2. Meanwhile, Cu(0.5 wt%)–Fe(0.5 wt%)/TiO_2–SiO_2–acac is found to improve the quantum yield and energy efficiency of methane production as compared to those of ethylene production. TiO_2–SiO_2–acac is observed to enhance the total energy efficiency of methane and ethylene production up to ca. 15% in comparison with using of bare TiO_2 counterpart.

The production rate of methane according to reaction time over bare TiO_2–SiO_2–acac and Cu(0.5 wt%)–Fe(0.5 wt%)/TiO_2–SiO_2–acac catalysts under UVA is

Table 4
Quantum yield (Φ) and energy efficiency (η) of ethylene and methane production over different catalysts under UVA

Photocatalyst	C_2H_4 evolution		CH_4 evolution		η_{total} (%)
	Φ (%)[a]	η (%)[a]	Φ (%)[a]	η (%)[a]	
Cu(0.5 wt%)–Fe(0.5 wt%)/TiO_2/optical fiber	0.0235	0.0084	0.0245	0.0075	0.0159
Cu(0.5 wt%)–Fe(0.5 wt%)/TiO_2–SiO_2–acac/optical fiber	0.0085	0.0030	0.0500	0.0152	0.0182

[a]One photon energy at 365 nm is 5.45×10^{-19} J. Photon energy absorbed by fibers is 17.4 mW (17.4×10^{-3} J/s). The total number of absorbed photons per second is 3.19×10^{16}.

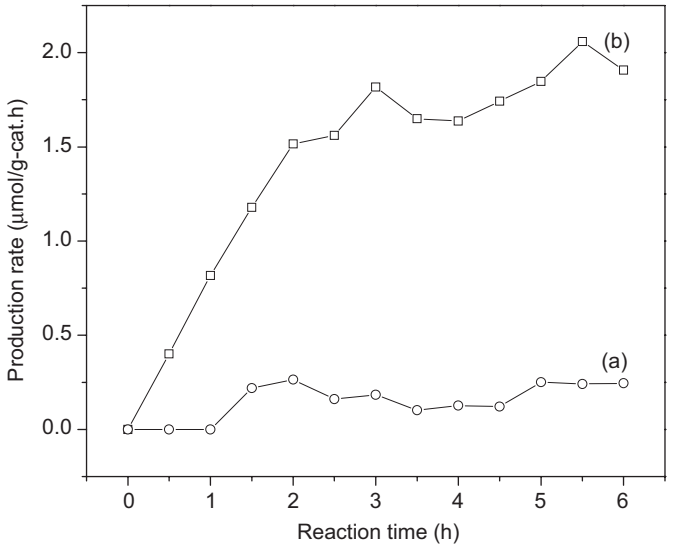

Fig. 8. Production rate of methane according to reaction time over (a) bare TiO_2–SiO_2–acac and (b) Cu(0.5 wt%)–Fe(0.5 wt%)/TiO_2–SiO_2–acac. The reaction was carried out under UVA (320–500 nm) with the intensity of 225 mW/cm^2. Photocatalysts were coated on 216 optical fibers.

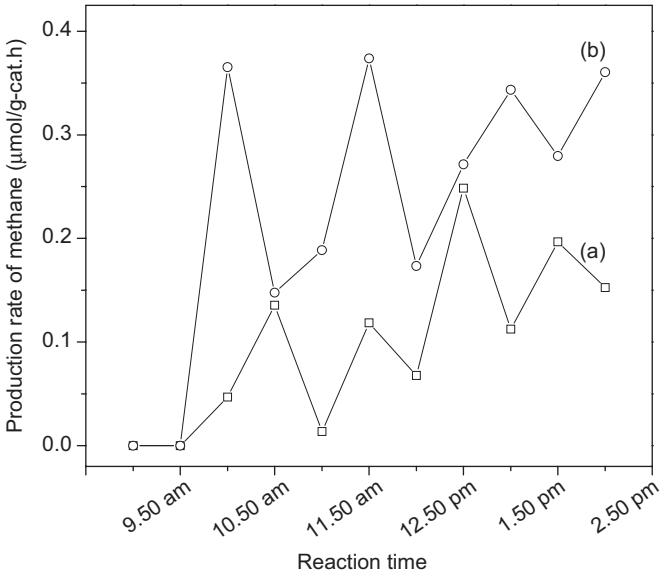

Fig. 9. Production rate of methane according to reaction time over (a) bare TiO_2–SiO_2–acac and (b) Cu(0.5 wt%)–Fe(0.5 wt%)/TiO_2–SiO_2–acac. The experiment for TiO_2–SiO_2–acac catalyst was carried out on May 11, 2007 from 9.30 am to 3.00 pm in Taipei, Taiwan under average solar light intensity of 6.35 mW/cm^2. The experiment for Cu(0.5 wt%)–Fe(0.5 wt%)/TiO_2–SiO_2–acac was carried out on May 12, 2007, from 10.30 am to 4.00 pm under average solar light intensity of 2.05 mW/cm^2. Photocatalysts were coated on 216 optical fibers.

shown in Fig. 8. The production rate of methane on Cu(0.5 wt%)–Fe(0.5 wt%)/TiO_2–SiO_2–acac catalyst substantially increases from the beginning until 2 h after turning on the light. Cu and Fe as dopants are found to some extent to stably maintain the production rate of methane at ca. 1.8 μmol/g-cat h up to 6 h after turning the light on.

Fig. 9 presents the photoactivities of bare TiO_2–SiO_2–acac and Cu(0.5 wt%)–Fe(0.5 wt%)/TiO_2–SiO_2–acac catalysts under concentrated sunlight versus daylight hours. In contrast to the reaction under UVA, production rate of methane under natural sunlight is significantly changed according to daylight hours, which results from the apparently unstable weather during the experimental day. Nevertheless, the superior photoactivity of Cu(0.5 wt%)–Fe(0.5 wt%)/TiO_2–SiO_2–acac as compared to that of bare TiO_2–SiO_2–acac catalyst under natural sunlight is consistent with the data under UVA as presented in Fig. 8.

3.3. Discussion

The specific surface areas of both TiO_2–SiO_2 and TiO_2–SiO_2–acac catalysts are found to be much higher than that of bare TiO_2 (P25). It was well known that the presence of SiO_2 in TiO_2 lattice results in the increase in specific surface area of derived TiO_2–SiO_2 [20,26,27]. This phenomenon could be ascribed to the amorphous phase of SiO_2 in the TiO_2–SiO_2 mixed oxide [20,26,27]. Furthermore, SiO_2 is also a material that is well agreed to increase the band-gap energy of derived TiO_2–SiO_2 mixed oxide, which is resulted from the formation of Ti–O–Si linkage [20,26,27]. Meanwhile, the addition of metals into TiO_2–SiO_2 lattice brings about the decrease in the specific surface area of resulting metal-doped TiO_2–SiO_2 catalyst. However, Cu and Fe metals doped on TiO_2–SiO_2 catalyst is found to shift the light absorption of the derived catalysts to visible range as shown in Fig. 5. Acetyl acetone (acac) as a chelating agent was deliberately employed in sol–gel process to reduce the hydrolysis as well as the condensation rates of TTIP and TEOS [28], resulting in the inherent

inserting of Fe metal into the TiO_2–SiO_2 lattice. As a consequence, metal-doped TiO_2–SiO_2–acac shows strong visible light absorption as compared to TiO_2–SiO_2 counterpart as presented in Fig. 5.

It is interestingly observed in Table 2 that under UVA bare TiO_2, TiO_2–SiO_2 and TiO_2–SiO_2–acac catalysts are not photoactive towards ethylene production. Meanwhile, they are found to produce methane under UVA, though TiO_2 only presents negligible photoactivity towards methane production. These results could be ascribed to the much low redox potential of methane as compared to that of ethylene [29]. Furthermore, the reduction potential of TiO_2–SiO_2 catalyst is also higher than that of TiO_2 counterpart [20,26,27]. When TiO_2 and TiO_2–SiO_2 are doped with Cu and Fe metals, the resulting catalysts show substantial difference in hydrocarbon production as well as product selectivity. TiO_2 as a support favors the production of ethylene, whereas methane evolution is significantly observed on TiO_2–SiO_2–based catalysts. It was well known that the electrochemical reduction of CO_2 on single-crystal copper electrodes formed various kinds of hydrocarbon products depending on its index planes [30–32]. In our previous report, Cu/TiO_2 catalyst was found to favorably reduce CO_2 with H_2O to methane rather than ethylene [22]. Meanwhile, although Fe as a co-dopant on Cu/TiO_2 catalyst was observed to give rise to the synergistic performance of CO_2 reduction to ethylene, it substantially decreased the photoactivity towards methane production [22]. Accordingly, the inherent inserting of Fe metal into the TiO_2–SiO_2 lattice in this present study would depress the effect of Fe on methane production, which gives rise to the significant production of methane on TiO_2–SiO_2-based catalysts.

On the other hand, only methane is produced on TiO_2–SiO_2–based catalysts under natural sunlight as depicted in Table 3. Although Cu and Fe as dopants are observed to improve the photoactivities of resulting catalysts including the presence of significant amount of ethylene in the products under UVA, they produce only methane under natural sunlight with the improved productivity. This result could be explained by negligible intensity of UVA in the sunlight, which is filtered out in the solar concentrator. According to the manufacturer, UVA is filtered out in order to protect the plastic optical fiber in the light-transmission cable. It is found in Tables 2 and 3 that bare TiO_2–SiO_2 catalyst supported on optical fiber only produces comparable amount of methane either under UVA with the intensity of 225 mW/cm^2 or under natural sunlight with the average intensity of 6.35 mW/cm^2. This phenomenon could infer that the increase in light intensity might not compensate the inherent electron-hole recombination in the TiO_2–SiO_2–acac catalyst. On the other hand, Cu–Fe/TiO_2–SiO_2–acac in Table 3 shows strong photo-productivity of methane as compared to that of bare TiO_2–SiO_2–acac, which could be resulted from the full absorption of visible light of this catalyst as shown in Fig. 5c.

4. Conclusions

The advantage of photo-driven reaction is clearly benefited from the un-limited solar energy. An optical-fiber reactor provides an efficient way to perform photo-driven reactions. Compared with a traditional packed-bed reactor, an optical fiber provides a medium to transmit light uniformly throughout a reactor. TiO_2–SiO_2 mixed oxide-based photocatalysts are synthesized and coated on the optical fibers in this present work to reduce CO_2 with H_2O to methane and ethylene under UVA as well as concentrated natural sunlight. The inserting of Fe metal into TiO_2–SiO_2 lattice is found to substantially promote the full visible light absorption of the resulting catalyst. This result also brings about the change of product selectivity of Cu–Fe/TiO_2–SiO_2 catalyst. Cu–Fe/TiO_2 catalyst is observed to enhance ethylene production, whereas methane is significantly evolved over Cu–Fe/TiO_2–SiO_2 counterpart. Full visible light absorption of Cu–Fe/TiO_2–SiO_2–acac catalyst is found to bring about the superior photo-productivity of methane as compared to that of bare TiO_2–SiO_2–acac counterpart under natural sunlight. An efficient photoreactor with high-photoactivity catalyst is essential step toward a commercial-scale application to produce renewable fuels.

Acknowledgments

The authors would like to acknowledge the National Science Council of Taiwan for financial supporting this research under Contract no. NSC 95-2911-I-002-088 and NSC 96-2120-M-002-017.

References

[1] M.R.M. Abu-Zahra, L.H.J. Schneiders, J.P.M. Niederer, P.H.M. Feron, G.F. Versteeg, Int. J. Greenhouse Gas Control 1 (2007) 37.
[2] A. Fridman, A. Gutsol, A. Dolgopolsky, E. Shtessel, Energy Fuels 20 (2006) 1242.
[3] A. Demirbas, Prog. Energy Combust. Sci. 33 (2007) 1.
[4] Z. Sen, Prog. Energy Combust. Sci. 30 (2004) 367.
[5] J. Hawecker, J.-M. Lehn, R. Ziessel, J. Chem. Soc. Chem. Commun. (1985) 56.
[6] K. Thampi, J. Kiwi, M. Grätzel, Nature 327 (1987) 506.
[7] H. Ishida, K. Tanaka, T. Tanaka, Chem. Lett. 6 (1987) 1035.
[8] V. Heleg, I. Willner, J. Chem. Soc. Chem. Commun. 18 (1994) 2113.
[9] T. Mizuno, K. Adachi, K. Ohta, A. Saji, J. Photochem. Photobiol. A: Chem. 98 (1996) 87.
[10] S. Kaneco, H. Kurimoto, K. Ohta, T. Mizuno, A. Saji, J. Photochem. Photobiol. A: Chem. 109 (1997) 59.
[11] H. Yoneyama, Catal. Today 39 (1997) 169.
[12] I.-H. Tseng, W.-C. Chang, J.C.S. Wu, Appl. Catal. B: Environ. 37 (2002) 37.
[13] G. Guan, T. Kida, T. Harada, M. Isayama, A. Yoshida, Appl. Catal. A: Gen. 249 (2003) 11.
[14] Y. Shioya, K. Ikeue, M. Ogawa, M. Anpo, Appl. Catal. A: Gen. 254 (2003) 251.
[15] G. Guan, T. Kida, A. Yoshida, Appl. Catal. B: Environ. 41 (2003) 387.
[16] I.-H. Tseng, J.C.S. Wu, H.-Y. Chou, J. Catal. 221 (2004) 432.
[17] I.-H. Tseng, J.C.S. Wu, Catal. Today 97 (2004) 113.

[18] J.C.S. Wu, H.-M. Lin, C.-L. Lai, Appl. Catal. A: Gen. 296 (2005) 194.
[19] T.-V. Nguyen, H.-C. Lee, O.-B. Yang, Sol. Energy Mater. Sol Cells 90 (2006) 967.
[20] T.-V. Nguyen, D.-J. Choi, O.-B. Yang, Res. Chem. Intermed. 31 (2005) 483.
[21] A. Danion, J. Disdier, C. Guillard, F. Abdelmalek, N. Jaffrezic-Renault, Appl. Catal. B: Environ. 52 (2004) 213.
[22] T.-V. Nguyen, J.C.S. Wu, Appl. Catal. A: General 335 (2008) 112.
[23] G. Pecchi, P. Reyes, T. López, R. Gómez, A. Moreno, J.L.G. Fierro, J. Chem. Technol. Biotechnol. 77 (2002) 944.
[24] H.V. Damme, G.A. Somorjai, Supports in photocatalysis and surface science of catalysis and photocatalysis, in: N. Serpone, E. Pelizzetti (Eds.), Photocatalyst-Fundamentals and Applications, Wiley, New York, 1989, 176, 299, 305.
[25] C.D. Wagner, W.M. Riggs, L.E. Davis, J.F. Moulder, G.E. Muilenberg, Handbook of X-ray Photoelectron Spectroscopy, Perkin-Elmer Corporation, Eden Prairie, 1978, 76–82.
[26] T.-V. Nguyen, O.-B. Yang, Catal. Today 87 (2003) 69.
[27] T.-V. Nguyen, S. Kim, O.-B. Yang, Catal. Commun. 5 (2004) 59.
[28] C.J. Brinker, G.W. Scherer, Sol–gel Science: The Physics and Chemistry of Sol–gel Processing, Academic Press, San Diego, 1990, 52–59.
[29] M. Gattrel, N. Gupta, A. Co, J. Electroanal. Chem. 594 (2006) 1.
[30] Y. Hori, I. Takahashi, O. Koga, N. Hoshi, J. Phys. Chem. B 106 (2002) 15.
[31] K.W. Frese Jr., Electrochemical reduction of CO_2 at solid electrodes, in: B.P. Sullivan, K. Krist, H.E. Guard (Eds.), Electrochemical and Electrocatalytic Reactions of Carbon Dioxide, Elsevier, Amsterdam, 1993, 191.
[32] Y. Hori, H. Wakebe, T. Tsukamoto, O. Koga, Surf. Sci. 335 (1995) 258.